High-content imaging characterization of cell cycle therapeutics through *in vitro* and *in vivo* subpopulation analysis

Jonathan Low,[1] Shuguang Huang,[2] Wayne Blosser,[1] Michele Dowless,[1] John Burch,[3] Blake Neubauer,[3] and Louis Stancato[1]

Departments of [1]Cancer Growth and Translational Genetics, [2]Statistics and Information Science, and [3]*In vivo* Pharmacology, Eli Lilly and Company, Indianapolis, Indiana

Abstract

Although the cycling of eukaryotic cells has long been a primary focus for cancer therapeutics, recent advances in imaging and data analysis allow even further definition of cellular events as they occur in individual cells and cellular subpopulations in response to treatment. High-content imaging (HCI) has been an effective tool to elucidate cellular responses to a variety of agents; however, these data were most frequently observed as averages of the entire captured population, unnecessarily decreasing the resolution of each assay. Here, we dissect the eukaryotic cell cycle into individual cellular subpopulations using HCI in conjunction with unsupervised K-means clustering. We generate distinct phenotypic fingerprints for each major cell cycle and mitotic compartment and use those fingerprints to screen a library of 310 commercially available chemotherapeutic agents. We determine that the cell cycle arrest phenotypes caused by these agents are similar to, although distinct from, those found in untreated cells and that these distinctions frequently suggest the mechanism of action. We then show via subpopulation analysis that these arrest phenotypes are similar in both mouse models and in culture. HCI analysis of cell cycle using data obtained from individual cells under a broad range of research conditions and grouped into cellular subpopulations represents a powerful method to discern both cellular events and treatment effects. In particular, this technique allows for a more accurate means of assessing compound selectivity and leads to more meaningful comparisons between so-called targeted therapeutics. [Mol Cancer Ther 2008;7(8):2455–63]

Received 4/4/08; revised 5/15/08; accepted 5/30/08.

The costs of publication of this article were defrayed in part by the payment of page charges. This article must therefore be hereby marked *advertisement* in accordance with 18 U.S.C. Section 1734 solely to indicate this fact.

Requests for reprints: Louis Stancato, 355 East Merrill Street, Dock 48 DC 0434, Indianapolis, IN 46225. Phone: 317-655-6910; Fax: 371-276-1414. E-mail: l.stancato@lilly.com

Copyright © 2008 American Association for Cancer Research.

doi:10.1158/1535-7163.MCT-08-0328

Introduction

Understanding the regulation and progression of the cell cycle is a critical component in combating a wide variety of human diseases, the most prominent being cancer (1, 2). Our current understanding of phenotypic changes during cell cycle progression is based on well-defined observations using classic flow cytometry, microscopy, and early forms of automated imaging, but few reports followed cellular subpopulations as they progressed through the cell cycle (3–5). Instead, these reports observed mixed populations of cells or were unable to perform subpopulation analysis, thereby generating an incomplete view of cell cycle progression (4, 5). Due to the nature of these previous investigations, which measured the average effects of a treatment on a population of cells, they were unable to resolve several factors including variability in the rate of cell cycle progression, response to treatment between cells, all-or-none effects, and events only occurring in rare subpopulations. Although measuring the average changes in cellular morphology or protein expression across a population gives a general idea of what is happening, it frequently lacks the resolution necessary to delve into advanced treatment of many current cellular questions and disease states. For instance, variation in cancer cells frequently leads to chemotherapeutic treatments that affect only a subpopulation of cells due to differences in gene expression, mutation, cellular signaling, or tumor microenvironment. When studying the deregulation of the cell cycle and potential treatments to kill these cells, it is vital to focus on subpopulations that can be affected by a given therapy to prevent recurrence and metastasis.

High-content imaging (HCI) is an increasingly important method of elucidating changes in cellular biology. The combination of validated immunofluorescent assays, availability of automated microscopy, and advances in image analysis software led to increased exploitation of this technology in a variety of settings ranging from cellular signaling pathways to drug discovery (6, 7). Recently, others have shown the advantages of HCI by revealing complex interactions between experimental molecules and cellular populations using several variables (8–10). These approaches easily identify active compounds and effective concentrations as well as distinguish classes of compounds from one another. Although HCI analysis of single variables can quantify treatment effects on each cell and lead to an improved understanding of how cells progress through the cell cycle, these results have most frequently been viewed as an aggregate response of the entire population (11). Although these single-variable analyses do not define every phase of the cell cycle, the incorporation of additional variables delineates multiple phases (5).

Downloaded from http://aacrjournals.org/mct/article-pdf/7/8/2455/1880320/2455.pdf by guest on 06 October 2022

The key to understanding and defining subpopulations of cells is multiparametric analysis using several relevant phenotypic variables in combination to refine the definition of each population and subpopulation at the level of individual cells.

Although HCI has rapidly advanced over the past decade, there are currently two primary limitations to this technology. First, most experiments continue to focus treatment effects on an entire population of cells and how one or two variables are affected in individual cells (6, 7, 9). In these experiments, the population of cells is viewed as giving a singular response rather than a combination of several subpopulations, all potentially responding differently to treatment. These differentially responsive subpopulations may play a major role in disease progression as is evident in cancer biology, where cancer stem cells may comprise <1% of the total tumor population but potentially drive recurrence, invasion, and metastasis (12, 13). The second limitation of HCI is the interpretation of the large amount of data generated. Observing changes over a range of time, treatments, and cellular settings with HCI produces extensive data sets requiring detailed analysis. To solve these issues, we developed informatics tools to characterize treatment effects both on the entire population and on individual cellular subpopulations to generate a phenotypic fingerprint of the cell cycle.

Due to the importance of the cell cycle in oncology research, we chose to further elucidate the mammalian cell cycle to illustrate the advantages of the high-content subpopulation analysis method. We show a phenotypic high-content fingerprint for each phase of the cell cycle, each further subdividable into higher-resolution clusters, and show that these phenotypic fingerprints are reproducible across mammalian cell lines *in vitro*. We illustrate that common cell cycle modulators result in phenotypes similar to those observed for each phase of the cell cycle and that variation in these phenotypes often suggest mechanism of action. Finally, we show that the cellular phenotypes seen on compound treatment in tissue culture are similar to those observed *in vivo* after intravenous infusion.

Materials and Methods

Cell Culture and Compound Treatment

Calu-6, MDA-MB-231, HCT-116, HeLa, U20S, and 293T cells were grown according to the American Type Culture Collection guidelines. For the assays described below, adherent cells were plated into poly-D-lysine-coated 24- or 96-well dishes (Becton Dickinson) at a density of 30,000 or 3,000 cells in 1 mL or 100 μL medium, respectively, as determined by a Coulter Z2 cell and particle counter. p388 suspension cells were grown in T-25 flasks at a density of 1,000,000 per 7 mL. A double thymidine block was used to synchronize HeLa cells as described previously (14). Bromodeoxyuridine (BrdUrd) was added to the cells at a final concentration of 10 μmol/L for 1 h before fixation. HeLa cells were incubated with compounds in a final concentration of 0.5% DMSO. Compound dilutions and additions were done in duplicate on multiple days using a Multimek-96 automated pipettor (Beckmann). Cultured p388 cells were treated with multiple cell cycle agents in a final concentration of 0.5% DMSO in duplicate on multiple days.

Female BDF1 mice were used to characterize the phenotype of p388 cells *in vivo*. The mice were inoculated i.p. with 1,250,000 viable p388 cells in medium lacking serum 72 h before compound treatment. Mice were then injected i.v. either with vincristine at 3.750 or 1.875 mg/kg in 0.9% saline or with 0.9% saline alone as vehicle control (3 mice per group). Twenty-three hours after treatment, mice were injected i.p. with 50 mg/kg BrdUrd. Twenty-four hours after treatment, p388 cells were harvested using gastric lavage. Cells were counted using a Beckman Coulter Vi-Cell XR cell viability counter, and a total of 100,000 viable cells were plated per condition. Cells were then centrifuged at 800 × *g* for 10 min and fixed and stained as below.

Immunofluorescence

Cells were fixed for 1 h at −20°C with 200 μL of an ice-cold solution containing 70% ethanol and 15 mmol/L glycine. All following dilutions were done in PBS at 25°C. Fixative was removed and each well washed with PBS. Cells were blocked using 1% bovine serum albumin (Invitrogen) for 1 h at 25°C. BrdUrd incorporation was detected using the Roche BrdUrd labeling and detection kit (Roche) as per the manufacturer's instructions. Fixation and BrdUrd detection was also done using the GE Healthcare Cell Proliferation and Fluorescence kit (GE Healthcare) after fixation with 3.7% formaldehyde for 20 min at 37°C and permeabilization with 0.1% Triton X-100 for 10 min at 25°C. The primary antibody against phospho-histone H3 (pHH3; Upstate Biolabs; ref. 15) was diluted in 1% bovine serum albumin to a final concentration of 5 μg/mL, and this mixture was added to each well for 1 h at 25°C. Each well was then washed three times with 200 μL PBS and incubated for 1 h at 25°C with a solution containing 5 μg/mL goat α-mouse Alexa 488 (Molecular Probes) to detect BrdUrd, 5 μg/mL goat α-rabbit Alexa 647 (Molecular Probes) to detect pHH3, and 200 ng/mL Hoechst 33342 to detect nuclear material (Molecular Probes) in 1% bovine serum albumin. Each well was then washed three times with 200 μL PBS and stored at 4°C until analysis.

Fluorescent Imaging and Statistical Analysis

Cell images were captured using a Cellomics Arrayscan VTI and analyzed with the Target Activation BioApplication reading in three channels at a magnification of ×10. Example images were captured at ×80 using a Zeiss Axiovert 200 M inverted fluorescent microscope. An algorithm was used to identify objects by nuclear staining with Hoescht dye, and the relative levels and subcellular localization of BrdUrd and pHH3 were determined through the respective intensities and locations of Alexa 488 and Alexa 647 fluorescence. A minimum of 1,000 individual cellular images or 20 fields were captured for each condition. For each cell, along with the intensity from

Downloaded from http://aacrjournals.org/mct/article-pdf/7/8/2455/1880320/2455.pdf by guest on 06 October 2022

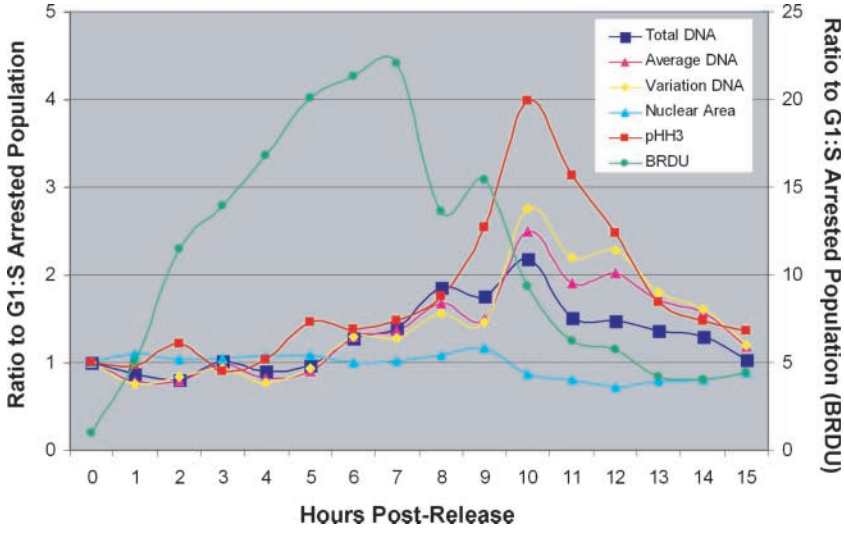

Figure 1. Well-level analysis of HeLa cell cycle progression. HeLa cells were synchronized by blocking DNA replication in early S phase. The cells were released from arrest and followed as they progressed through the cell cycle. The changes in the well-level averages of six phenotypic markers as the cells progressed through one replication cycle are displayed. All values are expressed as a ratio compared with HeLa cells arrested at the G_1-S transition. *Right,* BrdUrd incorporation ratio; *left,* all others.

each channel, several additional nuclear features were captured. The algorithm measured total nuclear area, the ratio of the perimeter of the nucleus compared with its area, and the length to width ratio of the nucleus. Arrayscan data were then transformed to a $\log_2$ format and further analyzed using unsupervised K-means clustering to group subpopulations with similar profiles in the studied variables (11, 16). All populations were compared with asynchronous untreated control populations on the same plate to account for plate-to-plate variation. Subpopulation clusters were derived from the entire population of a plate and intensities based on the SD away from the mean of the control population.

Results

Phenotypic Analysis

The Cellomics Arrayscan VTI was used to identify phenotypic changes as each cell progressed through the cell cycle. Because cell cycle progression is intimately tied to changes in nuclear DNA content, we first identified nuclear variables useful in defining a phenotypic fingerprint. Hoescht 33342 stain quantified four markers in each nucleus: the total amount of DNA, the nuclear area, the average DNA intensity per unit area, and the variation of DNA intensity (which measures uniformity of fluorescence across pixels). In addition to nuclear attributes, we assessed changes in two well-characterized cell cycle markers. To determine when cells were in mitosis, we measured the amount of pHH3 at the Ser^{10} position present in each cell. PHH3, phosphorylated by aurora B kinase, promotes recruitment of condensin to the chromosomes and is a marker for the chromosomal condensation present in mitosis (15, 17–20). To determine when cells were in S phase, we used the incorporation of BrdUrd into DNA as a marker of active DNA synthesis (21). Subpopulations were distinguished in distinct phases of the cell cycle through simultaneous changes across these six markers. Using unsupervised K-means clustering, we then determined how cell cycle progression or compound treatment shifted cells from one phase of the cell cycle to another.

Analysis of Whole Populations of Synchronous HeLa Cells

HeLa cells were synchronized in quadruplicate using a double thymidine block, released, and cultured for up to 15 h, whereupon time points were taken every hour (see Materials and Methods). Cells were then immunostained for BrdUrd incorporation, pHH3 expression, and nuclear morphology. Changes in the six phenotypic markers were plotted by pooling the data from all cells at each time point and comparing those data with that obtained from a population of cells synchronized at the G_1-S boundary (Fig. 1). As expected, BrdUrd expression increased >22-fold in S phase and decreased as the cells progressed into G_2. Expression of pHH3 remained low until nearly 8 h after release, corresponding to entry into mitosis. Changes in the total amount of DNA in the nuclei consisted of an expected 2-fold increase, corresponding to a 4N DNA content, which remained until 11 h after release, as the nuclei exited mitosis and returned to a 2N state. The nuclear area, already high from the block in early S phase, remained high throughout S phase and G_2 but decreased at 9 h after release as the cells condensed their nuclear material on entering mitosis. This condensation led to a rapid increase in average DNA intensity and variation of DNA intensity, both of which were first observed in late G_2, and remained elevated throughout mitotic division. At 13 h after release, the majority of cells had reached G_1 and were characterized by 2N DNA content, moderate nuclear area, low average and variation of DNA intensity, and no pHH3 expression or BrdUrd incorporation. Phenotypic characterization of the cell cycle at the well-level, or total population-level, confirmed that overall these six markers changed as expected. Although we followed changes in nuclear morphology and marker expression as the cells progressed through one cell cycle, measuring events using an average

Downloaded from http://aacrjournals.org/mct/article-pdf/7/8/2455/1880320/2455.pdf by guest on 06 October 2022

from all the captured cells left us unable to determine if all six of these variables changed in every cell or only in a subpopulation of those cells.

HeLa Cell Cycle Subpopulation Analysis

To better understand how the cellular subpopulations progressed after release from thymidine block, we used unsupervised K-means clustering to group the cells at each time point (Fig. 2). In all of the following heatmaps, the cells were sorted vertically within each cluster based on their total DNA intensity, with the individual cell variables displayed horizontally across the heatmap. Initially, cells were segregated into three clusters in an attempt to divide the population into the primary cell cycle compartments, G_1, S-G_2, and M with cells at each of the time points compared with a control population of asynchronous HeLa cells. Heatmap colors shifted to red denote an increase from the mean of the control, whereas colors shifted to blue indicate a decrease from the mean of the control. When a three-cluster heatmap of this asynchronous population was generated, we obtained distinct subpopulations of cells corresponding to the major populations at synchronized time points (Fig. 2A). Interestingly, although the majority of the cells were clustered in one subpopulation after synchronization, we found that double thymidine synchronization did not generate a uniform population. This variation in synchronization point is likely due to slow S-phase progression occurring as each cell approached the G_1-S boundary, was arrested with thymidine, and slowly replicated portions of its DNA while under arrest (14). These subpopulations remained evident in all replicates ($n = 4$) and experiments ($n = 6$). As we followed the HeLa cells through one division, we determined that these additional subpopulations were frequently either leading or lagging the major subpopulation. Nevertheless, the primary subpopulation was obvious at each stage of the cell cycle.

We first generated a fingerprint from cells arrested at the G_1-S boundary (Fig. 2B). These cells exhibit moderate amounts of total DNA as well as low average and variation of DNA intensities. Due to the G_1-S arrest, these 2N cells have nuclei nearly twice as large as the average of those found in an asynchronous population, indicative of nuclear size increase preceding DNA synthesis (5). As expected, BrdUrd incorporation and pHH3 expression were only detected at low levels in these cells. Those cells characterized as the major S-phase subpopulation (3 h after release; Fig. 2C) maintained enlarged nuclei with an increased total DNA content, generally less than 4N, while preserving relatively low average and variation of DNA intensity. DNA synthesis was highly elevated in these cells as evidenced by BrdUrd incorporation, whereas pHH3 expression levels remained low.

Eight hours after release, the majority of the HeLa cells were in the G_2 phase of the cell cycle (Fig. 2D) although relatively short as frequently occurs after a thymidine-mediated cell cycle arrest (14). Phenotypically, cells transitioning to G_2 retained some characteristics of cells in S phase while acquiring some aspects of cells in early mitosis. For example, the G_2 population contained a higher total DNA intensity compared with a S-phase population due to the completion of DNA synthesis. These cells also retained enlarged nuclei, whereas average DNA intensity and variation of DNA intensity increased in this population

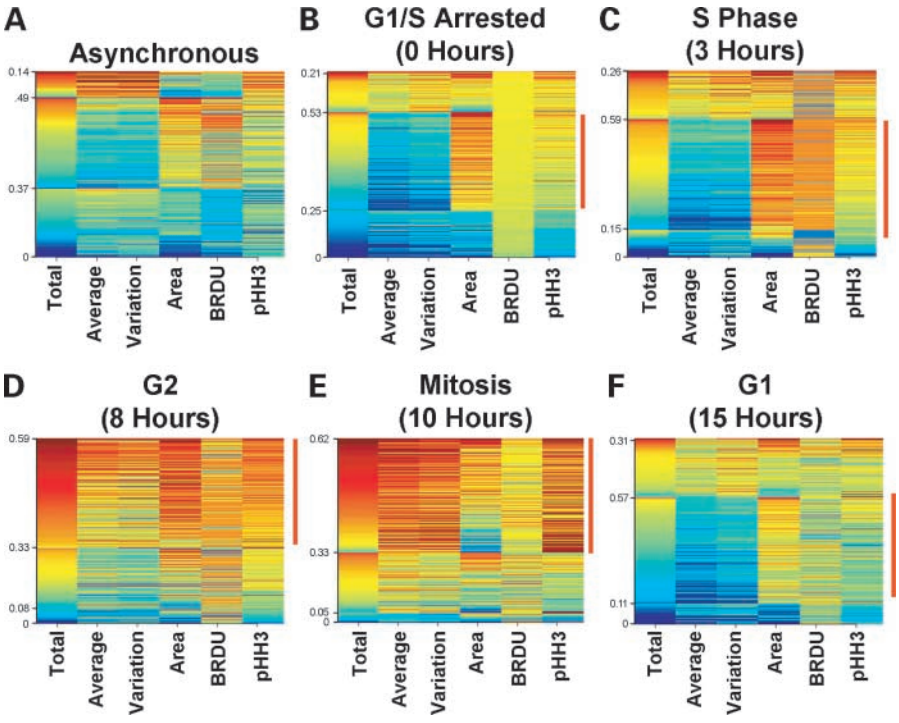

Figure 2. Multiparametric analysis defines subpopulations in each cell cycle compartment. The panels above were generated from the same experiment using the six variables shown in Fig. 1. The heatmaps above were created by clustering the data from each individual cell and sorting each cluster based on the total DNA intensity of the nucleus. The numbers on the left side of each heatmap denote the fraction of cells in each cluster. Distinct phenotypic fingerprints for asynchronous cells (**A**) and synchronized cells containing a major subpopulation showing a phenotype of cells at G_1-S (**B**), S phase (**C**), G_2 (**D**), mitosis (**E**), or G_1 (**F**) are illustrated. Total, average, and variation represent total DNA intensity, average DNA intensity, and variation of DNA intensity, respectively. Red lines to the side of each heatmap denote the cluster of interest.

Downloaded from http://aacrjournals.org/mct/article-pdf/7/8/2455/1880320/2455.pdf by guest on 06 October 2022

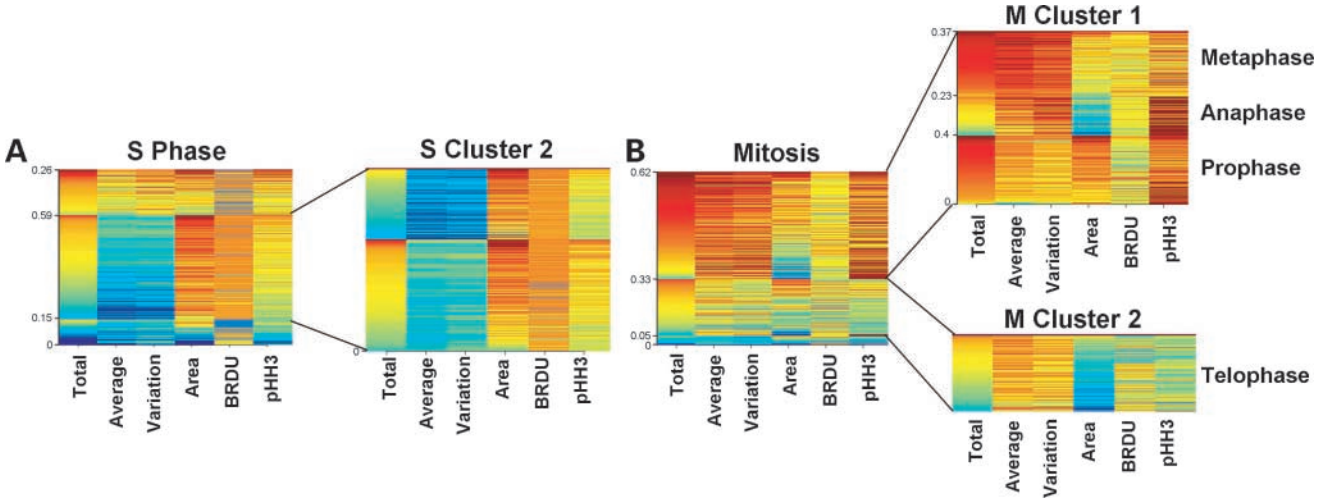

Figure 3. Subclustering major cell cycle compartments. Subclustering subpopulations formed from the initial analysis further distinguishes phenotypic populations. Two major S-phase clusters were detected on clustering cells with a S-phase phenotype corresponding to early and late S phase (**A**). All four major mitotic clusters were distinguished by subclustering two mitotic clusters (**B**). Prophase, metaphase, anaphase, and telophase were easily differentiated with distinct phenotypes.

due to changes in chromosome structure in preparation for mitosis (22). A low level of BrdUrd incorporation was detected in these cells, likely due to the incubation of these cells with BrdUrd for 1 h before fixation, and therefore capturing some residual DNA synthesis. The expression of pHH3 increased as these cells began chromosomal condensation and prepared to divide. Mitosis, which began at 9 h after release, was marked by a lack of BrdUrd incorporation, increased average DNA intensity, variation of DNA intensity, and pHH3 expression (Fig. 2E). Mitotic cells maintained relatively large nuclei, which rapidly condensed as they progressed into metaphase and beyond. At 12 h after release, we observed two distinct subpopulations of cells: one population of late mitotic cells in anaphase or early telophase and a second population of cells that had exited telophase and had entered early G_1. This G_1 population had low total DNA intensity, average DNA intensity, and variation of DNA intensity as well as relatively small nuclei and little pHH3 expression or BrdUrd incorporation. As the cells continued through G_1, they maintained all characteristics of an early G_1 population with the exception of slightly enlarged nuclei (Fig. 2F).

Subclustering Provides Greater Subpopulation Resolution

Determination of the exact cell cycle position can be a critical factor when deciding on a combination of targeted therapeutic agents or in differentiating activity between closely related molecules. For instance, a small amount of pHH3 was found in cells in cluster 2 at 3 h after release. On subclustering, we determined that there were in fact two discrete populations. The cells containing the higher average pHH3 and variation of DNA intensity progressed further in S phase than the subpopulation with less pHH3 and lower average and variation of DNA intensity (Fig. 3A). Even more powerful was the separation of all four major mitotic compartments using subpopulation analysis. Cells in cluster 1 at 10 h after release were subclustered into three clusters that corresponded to three of the four classic mitotic phases (Fig. 3B). The bottom cluster consists of cells in prophase, retaining relatively large nuclei, high total, average, and variation of DNA intensity, along with pHH3 expression and little BrdUrd incorporation. The top cluster consists of 4N cells that have begun to condense their nuclear material, resulting in increased average and variation of DNA intensity to levels even higher than those found in prophase. This metaphase cluster also contained high levels of pHH3. In the middle subpopulation, we detected cells in anaphase containing very small nuclei and 2N DNA but still retaining high average and variation of DNA intensity and intense pHH3 expression. To find cells in telophase, we subclustered cluster 2 of the 10 h after release heatmap. The telophase subpopulation detected in M cluster 2 contained a very small nuclear area with 2N DNA, high average and variation of DNA intensity, and little pHH3 expression. The dramatic changes in both total DNA intensity and pHH3 expression are the likely cause for telophase being clustered separately from the other three mitotic subpopulations. In each phase and subphase of the cell cycle, values obtained from individual cells were compared with the images of cells from those subpopulations to confirm that the heatmap analyses matched the classic phenotypes. Images with HCI morphology and intensity values representative of each stage of the cell cycle (Fig. 4A) were then matched with a heatmap showing the dominant HCI fingerprint for each of those stages (Fig. 4B), which allowed us to construct the HeLa cell cycle HCI fingerprint. We confirmed that phenotypes observed in HeLa cell cycle progression were found in other cancer cell lines (Supplementary Fig. S1).

Downloaded from http://aacrjournals.org/mct/article-pdf/7/8/2455/1880320/2455.pdf by guest on 06 October 2022

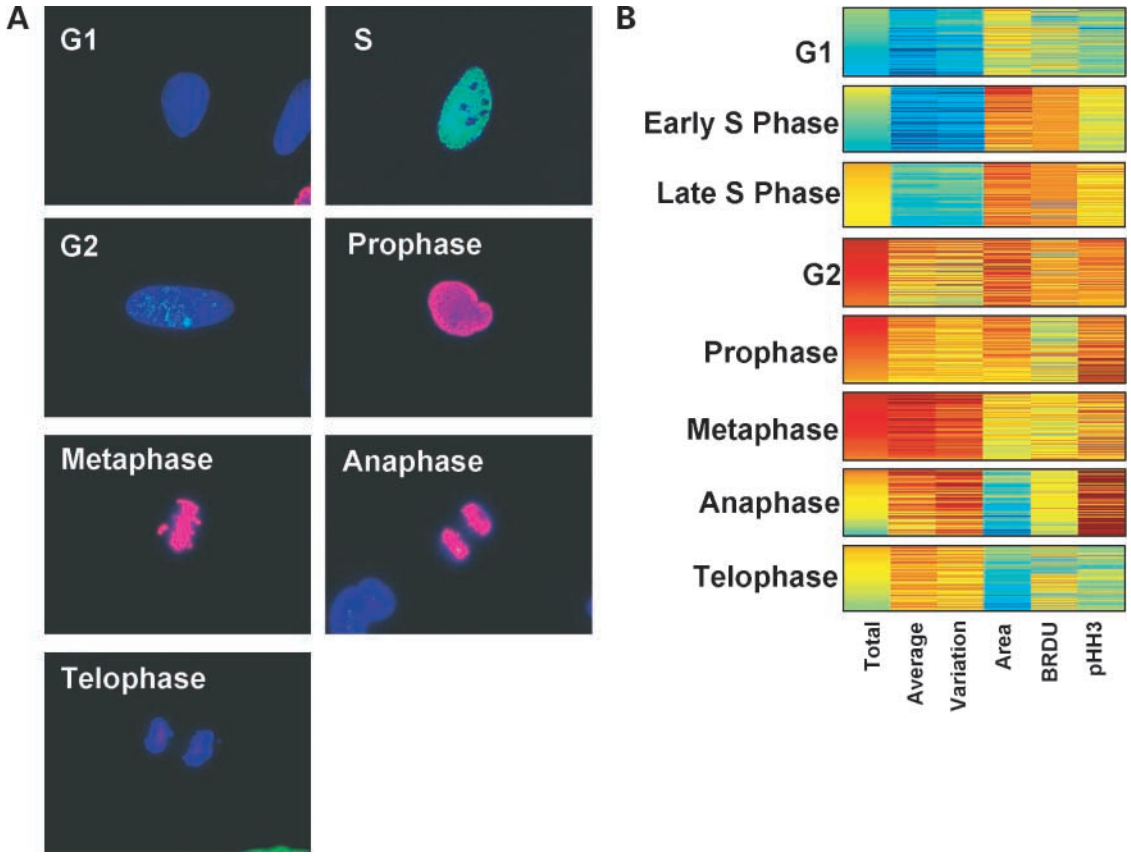

Figure 4. Key of cell cycle phenotypes and subpopulation heatmaps. Images were taken of each major cell cycle and mitotic phase at ×80 under standard HCI staining conditions (**A**). *Green fluorescence,* BrdUrd incorporation; *red fluorescence,* pHH3 expression. Heatmaps for cells at each stage of the cell cycle quantify the phenotypic differences found in these images (**B**).

Phenotypic Analysis of Commercial Oncolytics

To confirm the usefulness of subpopulation analysis in phenotypic drug discovery, we used the cell cycle assay to screen for the effects of 310 commercially available compounds in duplicate (Table 1). These compounds, from a variety of stages in the discovery process, were selected by choosing those with an indication for cancer and a known structure or known activity against at least one biological target. Although many of these compounds were not known cell cycle arrest agents and gave no effect, a significant number caused distinct forms of cell cycle arrest, with their phenotype matching the fingerprints of known cell cycle phases. First, we focused on how four compounds with well-understood cell cycle activity (nocodazole, paclitaxel, gemcitabine, and doxorubicin), but disparate mechanisms of action, affected HeLa cells (Fig. 5A). Although all four of these agents are known to increase DNA content, due to their activity in different cell cycle compartments, they were expected to generate distinctly different fingerprints. As expected, gemcitabine, a nucleoside analogue and inhibitor of thymidylate synthase and ribonucleotide reductase, and doxorubicin, an intercalating agent and inhibitor of topoisomerase II, inhibited the cell cycle in S phase; paclitaxel and nocodazole, which both inhibit proper microtubule function, blocked the cell cycle in mitosis (23–26). The phenotypes generated by these compounds were similar to, although distinct from, those found in untreated populations passing through S phase or mitosis. Although the phenotypes of the primary subpopulations of arrested cells were easily determined, there were dissimilarities between the cells

Table 1. Effects of 310 potential oncology compounds on the stage of cell cycle arrest

Phenotype	No. treatments with phenotype
Death	21
Death-S	10
Death-G_2	1
Death-M	5
G_1-S	1
S	25
M	10
No effect	237

Downloaded from http://aacrjournals.org/mct/article-pdf/7/8/2455/1880320/2455.pdf by guest on 06 October 2022

arrested with doxorubicin and gemcitabine, which help define the biology. Although both gemcitabine and doxorubicin increased the total DNA intensity and nuclear area, cells treated with doxorubicin had higher total and average DNA intensity than cells arrested with gemcitabine, suggesting that they were arrested later in S phase. These small changes in phenotypic fingerprints frequently suggested clues as to the mechanism of action of the compound. We also noted that a large increase in variation of DNA intensity without a corresponding increase in average DNA intensity frequently indicated cell death and corresponded to a decrease in cell number (Table 1). In cases of some highly potent compounds, the effects were such that cell cycle arrest phenotypes were masked by death of the treated populations. In other cases, cell death was evident along with cell cycle arrest phenotypes, whereas in others distinct cell cycle arrests were found without evidence of large-scale death.

As expected, most of the compounds had no discernable effect on the cell cycle, whereas those that did generated phenotypes based on compound target, phase arrest, and toxicity. For example, the DNA synthesis inhibitor herboxidiene generated a S-phase arrested phenotype but with very little BrdUrd incorporation. In contrast, methotrexate,

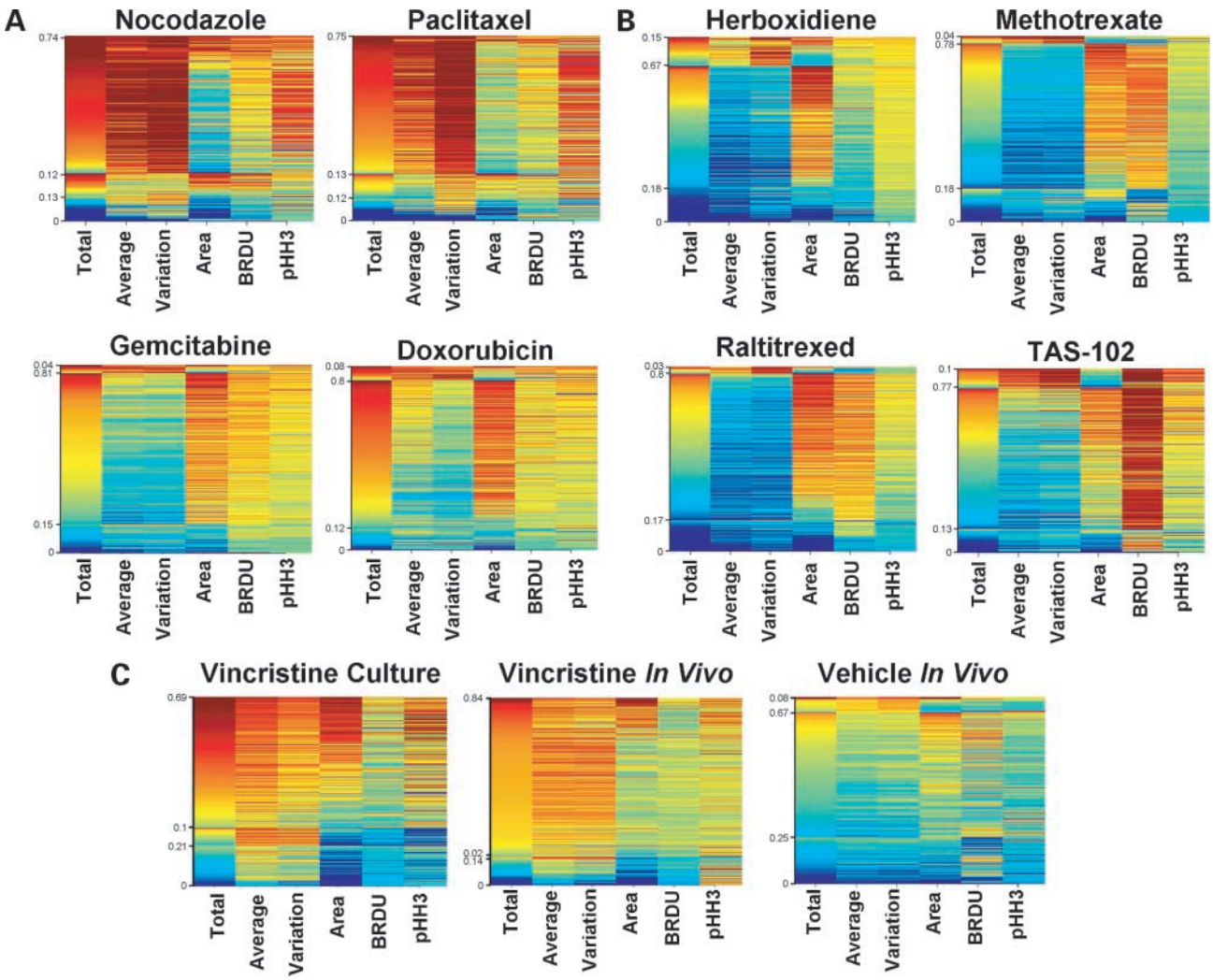

Figure 5. Compound treatments generate distinct and distinguishable phenotypes. HeLa cells were treated with the well-characterized agents nocodazole (125 nmol/L), paclitaxel (31 nmol/L), gemcitabine (62 nmol/L), and doxorubicin (125 nmol/L) to determine if arrest caused by compounds generated phenotypes similar to those in untreated cells (**A**). Cells were exposed to compounds for 48 h before exposure to BrdUrd, fixation, and marker detection. Nocodazole and paclitaxel generated phenotypes matching mitosis, whereas gemcitabine and doxorubicin produced S-phase phenotypes. HeLa cells were treated as above with the commercially available herboxidiene (1.67 μmol/L), methotrexate (185 nmol/L), raltitrexed (185 nmol/L), and TAS-102 (1.67 μmol/L; **B**). All four of these compounds created S-phase arrest phenotypes but can be distinguished phenotypically due to differences in arrest mechanism. p388 cells were treated with the mitotic agent vincristine in culture (20 nmol/L) or 72 h after inoculation into BDF1 mice (3.75 mg/kg). Cells were treated with vincristine or vehicle alone for 24 h before exposure to BrdUrd, fixation, and cell cycle marker detection (**C**). Treatment with vincristine generates similar phenotypes under both conditions.

Downloaded from http://aacrjournals.org/mct/article-pdf/7/8/2455/1880320/2455.pdf by guest on 06 October 2022

a folic acid reductase inhibitor, and raltitrexed, a thymidylate synthase inhibitor, also arrested cells in S phase, with a relatively high level of BrdUrd incorporation (Fig. 5B). Treatment with TAS-102, a thymidine phosphorylase inhibitor, clustered the majority of the population as a S-phase arrest but also induced far higher levels of BrdUrd incorporation than did gemcitabine-arrested or DMSO-treated cells (Fig. 5B). This phenotype is likely due to the low levels of biologically available thymidine caused by TAS-102 and thus decreasing competition for BrdUrd incorporation. In all cases, these compounds generated the expected subpopulation phenotypes for their expected phase of arrest.

In vivo Phenocopying of *In vitro* HCI Fingerprints

Establishment of HCI cell cycle fingerprints allows for classification of *in vitro* hit compounds that can then be advanced to *in vivo* tumor models, where efficacy is usually shown before advancement into human testing. Unlike cell culture, where compound concentration is tightly controlled and potential off-target effects (''polypharmacology'') are often mitigated, compound effects *in vivo* are often variable due to the many factors that affect compound exposure. Exposure levels either much higher or lower than needed to elicit an optimal *in vitro* response can effectively mask so-called on-target biology resulting in misinterpretation of *in vivo* activity. However, a focus on phenotypic outcomes that represent the sum of multiple cellular variables enables a richer, more detailed view of *in vivo* compound activity and should help to make more informed decisions regarding which compounds to advance, especially in following up phenotypic screening hits.

To address the need for a robust, high-throughput *in vivo* efficacy model for compounds targeting the cell cycle, we developed an *in vivo* HCI fingerprinting approach using the mouse p388 cell syngeneic macrophage leukemia model. Using this model, we characterized the effects of multiple cell cycle inhibitors in triplicate, including the microtubule-destabilizing agent vincristine (Fig. 5C), on cellular phenotype both *in vivo* and *in vitro* as described in Materials and Methods. In both cases, vincristine treatment in culture compared with i.v. bolus injection *in vivo* produced the expected mitotic block in the majority of the treated cells. Although there were minor differences in the intensities of the *in vivo* and *in vitro* samples, subpopulation analysis detected the major population in each case. Similar *in vitro* to *in vivo* phenocopying was noted for paclitaxel, and proprietary inhibitors against the kinesin family member EG5, or a multitargeted S-phase agent (*data not shown*). These data indicate the feasibility of monitoring phenotypic changes *in vivo* through the analysis of multiparametric HCI fingerprints.

Discussion

Although phenotypic changes in eukaryotic cells progressing through the cell cycle are relatively well defined, these changes were frequently observed singly or with two-dimensional flow cytometry. The use of HCI to visualize cellular events allows for multiplexing of seemingly independent readouts, but in spite of this ability HCI has most often been used as essentially a fluorescent plate reader displaying average effects on a total population. Subpopulation analysis of cell cycle images combines multiple cellular phenotypes to create a distinct fingerprint of cell cycle arrest. This method observes basic biology of cycling cells and classifies how a variety of perturbations affect groups of those cells through a combination of cellular variables that, as a whole, is much greater than the sum of its parts.

By directly comparing HeLa cells at both well and subpopulation levels, we determined that although the majority of cells express an expected phenotype, a small minority of cells can shift the interpretation of phenotypic expression patterns when observed as a whole. For example, although little BrdUrd labeling occurs outside of S phase, when HeLa cells were viewed as a single population, clusters of cells not synchronous with the major population gave the appearance that BrdUrd labeling occurred throughout the cell cycle. The discrimination between expressing and nonexpressing populations allows one to focus on the relevant subpopulations and the biology contained therein.

The cell cycle fingerprint generated in HeLa cells was applied to five additional cancer cell lines, and we confirmed that as these cell lines progressed through the cell cycle they followed similar patterns of phenotypic profiling. Importantly, although many of the variables varied widely between each of these cell lines, HCI subpopulation analysis generated a similar phenotypic cell cycle fingerprint and allowing for the development of a cell cycle fingerprint key (Fig. 4), applicable to cellular subpopulation analysis.

Analysis of >300 commercially available potential chemotherapeutic agents showed that subpopulation analysis detects compounds with cell cycle–specific effects and correctly identifies their phase of arrest. This analysis also confirmed that although many of these compounds have divergent mechanisms of action, those with cell cycle–specific effects were detected using HCI subpopulation analysis and those arrests were similar in phenotype to subpopulations found in untreated cells. Although many compounds assayed in this screen were not distinguished as being active, additional phenotypic analyses tailored to their mechanisms of action would likely detect the effects of these compounds.

There are two important advantages in using HCI subpopulation analysis to investigate cellular function. First, a perturbation in any of the multiple variables used to create a fingerprint of each cell cycle can change the interpretation of a population phenotype as a whole. These differing cell cycle fingerprints lead to a degree of sensitivity in this assay not found previously in HCI. As an example, although several compounds arrested the cell in S phase, this analysis distinguished between types of arrest within that phase due to divergent mechanisms of action. The HCI fingerprint of gemcitabine was

Downloaded from http://aacrjournals.org/mct/article-pdf/7/8/2455/1880320/2455.pdf by guest on 06 October 2022

distinguishable from those of methotrexate and TAS-102 due to differences in how the compounds affected DNA replication, although only one of the six phenotypic variables was affected. Distinguishing these subtle differences in cell cycle effects, and phenotypic effects in general, is one of the most powerful advantages of this system. Second, although slight phenotypic changes suggesting mechanisms of action are an advantage in many forms of analysis, the true power of this assay is the breakdown of each of the varying cellular subpopulations. Importantly, these tools are applicable to *in vivo* models and should aid in the identification of potential anticancer compounds that elicit desirable phenotypic effects such as cell cycle arrest, apoptosis, etc.

Importantly, HCI-based techniques support detection, resolution, and classification of phenotypes by a variety of agents that are masked when observing the cellular population as a whole. With these tools in place, the next step in molecular therapeutic classification is the two-dimensional organization of potential therapeutics based not only on chemical structure but also on biological fingerprint. The subpopulation analysis techniques used here to analyze the cell cycle can be applied to answer a wide variety of population-based cellular questions ranging from cancer endothelial cord formation to the characterization of subpopulations of stem cells. Characterizing the HCI phenotypes of cell cycle subpopulations is the first step to a better understanding of how cells act in a variety of disease states and respond to treatment in those same diseases.

Disclosure of Potential Conflicts of Interest

There are no conflicts of interest related to this publication or the work therein, although this work was done at Eli Lilly and Company.

Acknowledgments

We thank Mark Marshall, Mark Uhlik, the members of the Stancato laboratory, and the Lilly HCI statistics and informatics team for helpful discussions and advice.

References

1. Carnero A. Targeting the cell cycle for cancer therapy. Br J Cancer 2002;87:129 – 33.

2. Stewart ZA, Westfall MD, Pietenpol JA. Cell-cycle dysregulation and anticancer therapy. Trends Pharmacol Sci 2003;24:139 – 45.

3. Dormer P, Abmayr W. Correlation between nuclear morphology and rate of deoxyribonucleic acid synthesis in a normal cell line. J Histochem Cytochem 1979;27:188 – 92.

4. Kendall F, Swenson R, Borun T, Rowinski J, Nicolini C. Nuclear morphometry during the cell cycle. Science 1977;196:1106 – 9.

5. Nicolini C, Kendall F, Giaretti W. Objective identification of cell cycle phases and subphases by automated image analysis. Biophys J 1977;19: 163 – 76.

6. Lang P, Yeow K, Nichols A, Scheer A. Cellular imaging in drug discovery. Nat Rev Drug Discov 2006;5:343 – 56.

7. Moffat J, Sabatini DM. Building mammalian signalling pathways with RNAi screens. Nat Rev Mol Cell Biol 2006;7:177 – 87.

8. Loo LH, Wu LF, Altschuler SJ. Image-based multivariate profiling of drug responses from single cells. Nat Methods 2007;4:445 – 53.

9. Perlman ZE, Slack MD, Feng Y, Mitchison TJ, Wu LF, Altschuler SJ. Multidimensional drug profiling by automated microscopy. Science 2004; 306:1194 – 8.

10. Tanaka M, Bateman R, Rauh D, et al. An unbiased cell morphology-based screen for new, biologically active small molecules. PLoS Biol 2005; 3:e128.

11. Low J, Huang S, Dowless M, et al. High-content imaging analysis of the knockdown effects of validated siRNAs and antisense oligonucleotides. J Biomol Screen 2007;12:775 – 88.

12. Li F, Tiede B, Massague J, Kang Y. Beyond tumorigenesis: cancer stem cells in metastasis. Cell Res 2007;17:3 – 14.

13. Hambardzumyan D, Squatrito M, Holland EC. Radiation resistance and stem-like cells in brain tumors. Cancer Cell 2006;10:454 – 6.

14. Bostock CJ, Prescott DM, Kirkpatrick JB. An evaluation of the double thymidine block for synchronizing mammalian cells at the G_1-S border. Exp Cell Res 1971;68:163 – 8.

15. Hendzel MJ, Wei Y, Mancini MA, et al. Mitosis-specific phosphorylation of histone H3 initiates primarily within pericentromeric heterochromatin during G_2 and spreads in an ordered fashion coincident with mitotic chromosome condensation. Chromosoma 1997;106:348 – 60.

16. Venables WN, Ripley BD. Modern applied statistics. 4th ed. New York: Springer; 2002.

17. Gurley LR, Walters RA, Barham SS, Deaven LL. Heterochromatin and histone phosphorylation. Exp Cell Res 1978;111:373 – 83.

18. Preuss U, Landsberg G, Scheidtmann KH. Novel mitosis-specific phosphorylation of histone H3 at Thr^{11} mediated by Dlk/ZIP kinase. Nucleic Acids Res 2003;31:878 – 85.

19. Giet R, Glover DM. Drosophila aurora B kinase is required for histone H3 phosphorylation and condensin recruitment during chromosome condensation and to organize the central spindle during cytokinesis. J Cell Biol 2001;152:669 – 82.

20. Johansen KM, Johansen J. Regulation of chromatin structure by histone H3S10 phosphorylation. Chromosome Res 2006;14:393 – 404.

21. Yamada K, Semba R, Ding X, Ma N, Nagahama M. Discrimination of cell nuclei in early S-phase, mid-to-late S-phase, and G(2)/M-phase by sequential administration of 5-bromo-2′-deoxyuridine and 5-chloro-2′-deoxyuridine. J Histochem Cytochem 2005;53:1365 – 70.

22. Schor SL, Johnson RT, Waldren CA. Changes in the organization of chromosomes during the cell cycle: response to ultraviolet light. J Cell Sci 1975;17:539 – 65.

23. Huang P, Chubb S, Hertel LW, Grindey GB, Plunkett W. Action of 2′,2′-difluorodeoxycytidine on DNA synthesis. Cancer Res 1991;51: 6110 – 7.

24. Spadari S, Pedrali-Noy G, Focher F, et al. DNA polymerases and DNA topoisomerases as targets for the development of anticancer drugs. Anticancer Res 1986;6:935 – 40.

25. De Brabander M, De May J, Joniau M, Geuens G. Ultrastructural immunocytochemical distribution of tubulin in cultured cells treated with microtubule inhibitors. Cell Biol Int Rep 1977;1:177 – 83.

26. Schiff PB, Horwitz SB. Taxol stabilizes microtubules in mouse fibroblast cells. Proc Natl Acad Sci U S A 1980;77:1561 – 5.

Downloaded from http://aacrjournals.org/mct/article-pdf/7/8/2455/1880320/2455.pdf by guest on 06 October 2022